Classification of artificial light sources and estimation of Color Rendering Index using RGB sensors, K Nearest Neighbor and Radial Basis Function

J.-S. Botero V.[1,*], F.-E. López G.[1], J.-F. Vargas B.[2]

[1] Grupo AEyCC, Facultad de Ingenierías, Instituto Tecnológico Metropolitano ITM, Carrera 31 No. 54-10, Medellín, Colombia

[2] Grupo SISTEMIC, Facultad de Ingenierías, Universidad de Antioquia UdeA, Calle 70 No. 52-21, Medellín, Colombia

E-mail: juanbotero@itm.edu.co, franciscolopez@itm.edu.co, jesus.vargas@udea.edu.co

Submitted: May 15, 2015 ***Accepted: July 25, 2015*** ***Published: Sep. 1, 2015***

Abstract- Three types of artificial light sources work with electricity: incandescent, fluorescent and LED. These sources require characterization processes to allow selecting the most suitable for the application, to evaluate their capacity or more recently to tune and adjust their replicability using control algorithms. Therefore, it has been necessary to develop indices that represent these capabilities. The Color Rendering Index (CRI) is a measure used to characterize the color reproducibility of a light source in comparison to an ideal light source. The Correlated Color Temperature (CCT) is used to characterize light sources by representing the color as the temperature of a black body in Kelvin that shows nearly the same chromaticity as the analyzed light source. Using spectral information to determine the values in the XYZ space and deriving the calculation described in the standard is the best way to estimate the value of the CCT and the CRI. In this work, we implement a method to classify light sources and to select an estimation model of the CRI and the CCT using a low cost RGB sensor. The model estimation has been developed in this work and a separated algorithm for each source type has been built. The results show that using a K-Nearest Neighbor classifier, the error resulted less than $3.6%$. The error of the model estimation for the LED was 1.8%, for fluorescent light sources 0.09% and 1.2% for incandescent light sources.

Index terms*:* Color Rendering Index, CRI, light sources, Correlated Color Temperature, CCT, K Nearest Neighbor, Radial Basis Function, RBF, RGB sensors.

I. INTRODUCTION

Artificial light sources represent a technological frontier and since their invention, they offered humanity new points of view. Later, with the arrival of electricity began a new developmental path, seeking to increase their energy efficiency, lifetime and quality. There are three types of artificial sources: incandescent, fluorescent and LED. Incandescent light sources produce light by means of a wire filament heated to high temperatures, i.e. they emit electromagnetic radiation in the visible spectrum due to an electric current passing through them. Incandescent sources are energetically inefficient because large amounts of energy are converted into infrared radiation. The fluorescent lamps, which contain chemical compounds called phosphors, emit light using the effect of fluorescence. These chemicals emit visible light when they get excited by ultraviolet radiation. Fluorescent lamps are more efficient than incandescent lamps; however, some models find negative effects that affect the electrical network. Moreover, the LED lamps (Light-Emitting Diode) are the latest in lighting technology, based on the mechanism of electroluminescence in semiconductor materials. When electrons circulate the LED and pass the gap from the conduction band to the valence band of the atoms, they liberate energy in the form of a photon. According to the ``2010 U. S. Lighting Market Characterization'' developed for the U.S. Department of Energy by Navigant Consulting [1], the 19 % of electricity consumed in 2010, the equivalent to 700 TWh, in the United States is used by light sources, of these, 175 TWh were used in residences and 349 TWh in commercial environments.

Light plays a fundamental role in the interpretation of color. Objects reflect it and the receptors in the retina absorb it to generate our perception of color. Progress has been made building mathematical models that describe color and light sources. The most important are those made by the International Commission on Illumination (CIE for its acronym in French). Light sources play a key role in color perception, without light there is no color and, therefore, it is important to find characterization models. One measure to characterize light sources is the Color Rendering Index (CRI) [2]. The CRI is a measure used to characterize the ability of a light source to reveal the color of an object realistically compared to an ideal or natural source of light; but the use of this index is still under discussion and work has been done to compare it with more complex indices [3].

Another measure to characterize color is the Correlated Color Temperature (CCT) [4]. The CCT is used to characterize light sources by representing the color as the temperature of a black body in Kelvin that shows nearly the same chromaticity as the analyzed light source. There are several revisions from the original model [5], and some applications [6]. The best way to estimate the value of a CCT source is using the spectral information to determine the values in XYZ space. The values presented in [7] are used to convert the chromaticity coordinates, followed by using the defined reference point and the polynomial to calculate the CCT value. With the CCT and the CRI a set of mathematical descriptors can be obtained, which represent the light source. In addition, its direct relation to color is useful in the reconstruction of color models, and useful in many applications [8–10], just as RGB sensor or photodetectors applications [6,11–16].

If one considers spectrometry, it is difficult to implement the model and this complicates its use in common applications as dynamic lighting control [17–19], but the usefulness of adding controlled CCT-CRI models to such systems is indisputable. However, this implies the acquisition of SPD (Spectral Power Distribution), which is an economically expensive process.

Previously we developed a linear model to estimate the CCT with a limited set of SPD, with an error close to 6 % [20]. Similarly, we developed an estimation for the CRI [21] with a subset of SPD used in [20]; in this case the estimation error was also close to 6 %. The error in both models and the apparent non-linearity between the SPD and the measurements, led us to find solutions to reduce the error. Initially, it took the SPD again, in total 54, 34 of LED light sources, 16 of incandescent light sources and 6 of fluorescent light sources. The spectral proximity of sources of the same class (although obtained from different manufacturers) showed that the best option was building a model for each one; however, it was necessary to solve the problem of automatic classification. In this work, we implement a method for the classification of light sources and then select a model estimation of the CRI and the CCT using a low cost RGB sensor. The estimation model was also developed in this work and was necessary to build a separate algorithm for each type of light source. The results show that using a K-Nearest Neighbor classifier produced an error between 2.47 % and 4.44 % and an error of the estimation model for the LEDs between 1.24 % and 4.95 %. The error obtained with the Radial Basis Function (RBF) who have demonstrated their use in many areas [22,23], was between 0.00 % and 4.84 % for fluorescent light sources and 0.17 % and 1.2 % for incandescent light sources.

In the ``Materials and Methods" section some characteristics of the RGB sensors are described, subsequently the calculation model for the CCT and the CRI using the SPD is shown, and finally the architecture of the RBF model is presented. In the ``Results" section, some information about the database acquisition is shown and the error analysis for the classifier, as well as the individual regression models, are presented. The final part of this work draws conclusions.

II. MATERIALS

a. Color Sensors

TCS3414CS

The TCS3414CS is a color sensor manufactured by Texas Advanced Optoelectronic Solutions (TAOS). It is comprised of an 8x2 array of filtered photodiodes, four of which have red filters, four blue, and four green, the remaining four are not filtered, as shown in Figure 1. Each of the four sensor channels (Red, Green, Blue, and Clear) delivers its output in a format of 16 bits using I2C protocol information at 400 KHz. The gain of the analog converter and the integration time are programmable. The sensor has a synchronization input (SYNC), which allows the precise controlling of the integration of external sources. Figure 1 shows a magnified image of the sensor.

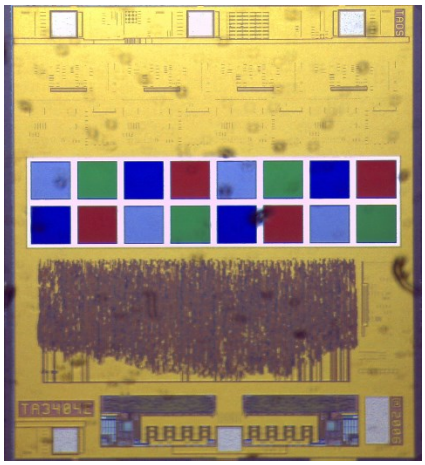

Figure 1. Microscopy image TCS3414CS

Table 1 shows some important features of the TCS3414CS color sensor. An internal filter eliminates the signal fluctuation caused by AC lighting flicker. An external capacitor is not needed.

Table 1. Characteristic TCS3414CS

Characteristic	*Value*	*Units*
Sensor	*Photodiode*	$[NA]$
Clock frequency	$0 - 400$	$[KHz]$
A/D Resolution	16	$[bits]$
Operating voltage	$2.7 - 3.6$	$[V]$
Supply Current ($V_{DD} = 3.6$)	*8.7-11*	$[mA]$
Operating temperature	$-40 - 85$	$[°C]$
Communication	*I2C*	$[NA]$
Chanels	*R, G, B, clear*	$[NA]$

ADJDS311

The ADJDS311 is a color sensor manufactured by Avago Technologies. This one is made of a 7x6 array of filtered photodiodes, ten of which have red filters, ten blue ones, and ten green ones, the remaining ten are not filtered, as shown in Figure \ref{fig:ADJDS311}. Each one of the four sensor channels (Red, Green, Blue, and Clear) delivers its output in a format of 10 bits using I2C protocol information at 100 KHz. The sensitivity is controlled control via a serial interface and can be optimized for the different color channel. Figure \ref{fig:ADJDS311} shows a magnified image of the sensor.

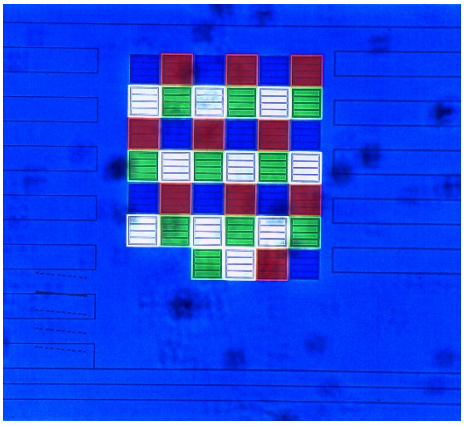

Figure 2. Microscopy image ADJDS311

Table 2 shows some important features of the ADJDS311 photo sensor. The sensor can be used in conjunction with a white LED for measuring the color on surfaces. It does not need an external capacitor.

Table 2. Characteristic TCS3414CS

Characteristic	*Value*	*Units*
Sensor	*Photodiode*	$[NA]$
Clock frequency	$0 - 100$	$[KHz]$
A/D Resolution	10	$[bits]$
Operating voltage	$2.7 - 3.6$	$[V]$
Supply Current ($V_{DD} = 3.6$)	*3.8-5*	$[mA]$
Operating temperature	$0 - 70$	$[°C]$
Communication	*I2C*	$[NA]$
Chanels	*R, G, B, clear*	$[NA]$

b. CIE standard observer matching functions

The CIE $\tilde{x}(\lambda)$, $\tilde{y}(\lambda)$, y $\tilde{z}(\lambda)$ color matching functions are curves numerically representing the response of an observer, as shown in Figure 3. These functions can be regarded as the spectral sensitivity curves of three linear light detectors, which produce the CIE tri-stimulus values X, Y and Z. This set of functions is known as the Standard Observer. [24] shows defined CIE standard colorimetric observer tables that were used for the calculations in this article.

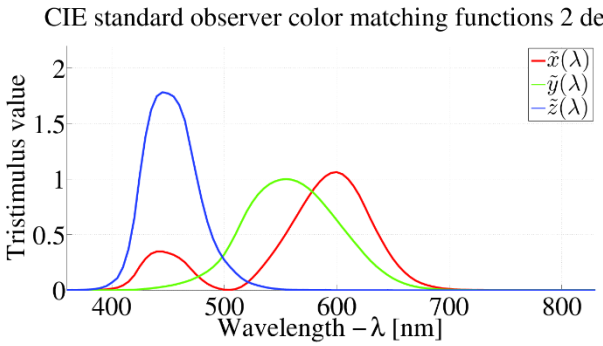

Figure 3. CIE Standard Observer color matching functions

CCT and CRI calculation

The CIE X, Y and Z coordinates of a light source can be calculated using the Spectral Power Distribution (SPD) of the light source and the CIE Standard Observer matching functions. The equations are presented in (1) where K is a constant for normalized Y a 100.

$$X = K \sum_{\lambda=380}^{780} SPD(\lambda) \cdot \tilde{x}(\lambda)$$
$$Y = K \sum_{\lambda=380}^{780} SPD(\lambda) \cdot \tilde{y}(\lambda) \quad (1)$$
$$Z = K \sum_{\lambda=380}^{780} SPD(\lambda) \cdot \tilde{z}(\lambda)$$

The chromaticity coordinates x, y can be obtained from X, Y y Z values. These equations are presented in (2).

$$x = \frac{X}{X+Y+Z}$$
$$y = \frac{Y}{X+Y+Z} \quad (2)$$

Later, with the equations shown in [7], the Correlated Color Temperature (CCT) is estimated. The equations are presented in (3).

$$n = \frac{x - 0.3320}{0.1858 - y}$$
$$CCT = 449n^3 + 3525n^2 + 6823n + 5520 \quad (3)$$

The next step is to determine the reference illumination based on the CCT of the light source. The reference light has the same CCT as the light source of interest, which is calculated using equation (4) if the value of CCT < 5000 K or using the model presented in (5), if otherwise. In (5), h is the Planck constant, c is the light speed, k is the Boltzmann constant and λ is the wavelength.

$$SPD_{Ref} = \frac{2\pi hc^2 \left(10^{-9}\lambda\right)^{-5}}{e^{\left(\frac{hc}{CCT \cdot 10^{-9} \lambda k}\right)} - 1} \quad (4)$$

For CCT $\geq$ 5000 K, the reference light can be calculated as shown in (5), where $S_0(\lambda)$, $S_1(\lambda)$ and $S_2(\lambda)$ are vectors of the distribution of daylight.

$$
\begin{aligned}
&SPD_{Ref}(\lambda) = S_0(\lambda) + \left[M_1 \cdot S_1(\lambda)\right] + \left[M_2 \cdot S_2(\lambda)\right] \\
&M_1 = \frac{-1.3515 - 1.7703 \cdot x_D + 5.9114 \cdot y_D}{0.0241 + 0.2562 \cdot x_D - 0.7341 \cdot y_D} \\
&M_2 = \frac{0.0300 - 31.4424 \cdot x_D + 30.0717 \cdot y_D}{0.0241 + 0.2562 \cdot x_D - 0.7341 \cdot y_D} \\
&CCT \leq 7000K \\
&x_D = -\frac{4.6070 \cdot 10^9}{T_C^3} + \frac{2.9678 \cdot 10^6}{T_C^2} + \frac{0.09911 \cdot 10^3}{T_C} + 0.244063 \\
&7000K < CCT \leq 25000K \\
&x_D = -\frac{2.0064 \cdot 10^9}{T_C^3} + \frac{1.9018 \cdot 10^6}{T_C^2} + \frac{0.24748 \cdot 10^3}{T_C} + 0.237040 \\
&y_D = -3.000 \cdot x_D^2 + 2.870 \cdot x_D - 0.275
\end{aligned}
\tag{5}
$$

Then the values of CIE 1960 (u, v) are determined for each of the eight color samples (TCS), both as a source of interest and as the reference illumination values for each $(X, Y \text{ and } Z)$,as shown in (6).

$$
\begin{aligned}
X_i &= K \sum_{\lambda=380}^{780} SPD(\lambda) \cdot \tilde{x}(\lambda) \cdot TCS_i(\lambda) d\lambda \\
Y_i &= K \sum_{\lambda=380}^{780} SPD(\lambda) \cdot \tilde{y}(\lambda) \cdot TCS_i(\lambda) d\lambda \\
Z_i &= K \sum_{\lambda=380}^{780} SPD(\lambda) \cdot \tilde{z}(\lambda) \cdot TCS_i(\lambda) d\lambda
\end{aligned}
\tag{6}
$$

Now the CIE 1960 (u, v) values are derived for each TCS using (8).

$$
\begin{aligned}
u &= \frac{4X}{X + 15Y + 3Z} \\
v &= \frac{6X}{X + 15Y + 3Z}
\end{aligned}
\tag{7}
$$

The adaptive color shift Von Kries is applied to respect the differences between the states of the chromatic adaptation of the light source of interest and the reference illumination as shown in (8). The c and d values are calculated for all the reference sources.

$$
\begin{aligned}
c &= \frac{1}{v}(4 - u - 10v) \\
d &= \frac{1}{v}(1.708v + 0.404 - 1.481u) \\
u_{k,i} &= \frac{10.872 + 0.404\frac{c_{ref}}{c_k}c_{k,i} - 4\frac{d_{ref}}{d_{k,i}}d_{k,i}}{16.518 + 1.481\frac{c_{ref}}{c_k}c_{k,i} - \frac{d_{ref}}{d_{k,i}}d_{k,i}} \\
v_{k,i} &= \frac{5.520}{16.518 + 1.481\frac{c_{ref}}{c_k}c_{k,i} - \frac{d_{ref}}{d_{k,i}}d_{k,i}}
\end{aligned}
\tag{8}
$$

Now, the CIE 1964 U*W*V values are determined for each TCS (9).

$$
\begin{aligned}
W_i^* &= 25(Y_i)^{1/3} - 17 \\
U_i^* &= 13(W_i)(u_i - u) \\
V_i^* &= 13(W_i^*)(v_i - v)
\end{aligned}
\tag{9}
$$

Finally the color shift is determined ΔE for each TCS, using the equation (10).

$$
\Delta E_i = \sqrt{(U_{ref,i}^* - U_{k,i}^*)^2 + (V_{ref,i}^* - V_{k,i}^*)^2 + (W_{ref,i}^* - W_{k,i}^*)^2} \tag{10}
$$

And with these values of ΔE the R_i and average CRI (11) are calculated.

$$
\begin{aligned}
R_i &= 100 - 4.6\,\Delta E \\
CRI = R_a &= \frac{1}{8}\sum_{1}^{8} R_i
\end{aligned}
\tag{11}
$$

c. Radial Basis Function RBF

The Neural Networks with Radial Basis Function are commonly built of two layers. These have been widely used to approximate functions and to linearize sensors [25]. A hidden layer consists of radial functions, and an output layer performs a weighted sum of the output from the hidden layer. The output of the hidden layer has the form shown in equation (12).

$$D = [d(m_{i,}c_1) \quad d(m_{i,}c_2) \quad d(m_{i,}c_3) \quad \cdots \quad d(m_{i,}c_n)] \tag{12}$$

In equation (12) m_i is the set of input variables, c_1, c_2, ..., c_n are multidimensional centroids estimated using the k-means algorithm and $d(m_{i,}c_1)$ denotes a function of the radial distance between the sample m_i and the c_j centroid. Note that the vector D resulting from the hidden layer is of dimension $[1xn]$, where n is the number of centroids as shown in Figure 4.

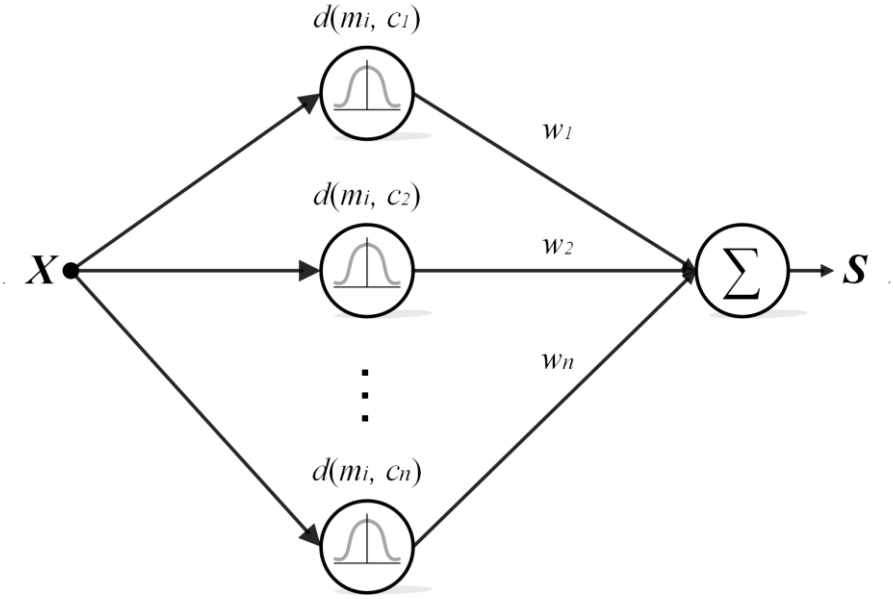

Figure 4. RBF architecture

The output layer can be expressed as shown in equation (13). Where D is the distance vector obtained from the hidden layer, W is the weight vector of the output layer obtained from the training algorithm and CRI_i is the output of $[1xn]$ dimension.

$$CRI_i = D_i \cdot W = [d(m_i,c_1) \quad d(m_i,c_2) \quad d(m_i,c_3) \quad \cdots \quad d(m_i,c_n)] \cdot \begin{bmatrix} w_1 \\ w_2 \\ w_3 \\ \vdots \\ w_n \end{bmatrix} \tag{13}$$

To train the output layer in the RBF network, it is necessary to find the solution that fits the system shown in (14) best. The rows of D in the equation (14) are constructed with the output of the hidden layer (D_i), where the number of rows is defined by the number of the training samples. The number of centroids n is estimated with k-means iterating to reduce the error value required by the application.

$$\begin{bmatrix} CRI_i \\ CRI_2 \\ CRI_3 \\ \vdots \\ CRI_n \end{bmatrix} = D \cdot W = \begin{bmatrix} d(m_1,c_1) & d(m_1,c_2) & d(m_1,c_3,) & \cdots & d(m_1,c_n) \\ d(m_2,c_1) & d(m_2,c_2) & d(m_2,c_3) & \cdots & d(m_2,c_n) \\ d(m_3,c_1) & d(m_3,c_2) & d(m_3,c_3) & \cdots & d(m_3,c_n) \\ \vdots & \vdots & \vdots & \ddots & \vdots \\ d(m_m,c_1) & d(m_m,c_2) & d(m_m,c_3) & \cdots & d(m_m,c_n) \end{bmatrix} \cdot W \tag{14}$$

The pseudo-inverse is used to solve this system. Pre-multiplying the transpose of D in equation (14) gives equation (15).

$$D^T \cdot CRI = D^T \cdot D \cdot W \tag{15}$$

Solving for W, the projection of the vector W is obtained in the column space of D. It is shown in equation (16). Given that $D^T \cdot D$ matrix is symmetric, the system is always invertible and therefore always has a solution.

$$\widetilde{W} = (D^T \cdot D)^{-1} \cdot D^T \cdot CRI \tag{16}$$

III. SOLUTION

a. Acquisition

The database consists of 54 records (SPD), of these, 34 correspond to LED sources, 14 to incandescent light sources and 6 to fluorescent light sources. The chosen light sources are from different manufacturers, including Osram, General Electric, Philips, and Sylvania. The measured CRI (which was estimated with calculus) varied between 59 and 99 and the CCT between 2300 K

and 6200 K. Figure 5 shows four SPD samples of fluorescent light sources characterized by peaks. The minimum CRI was 59 and the maximum 93.

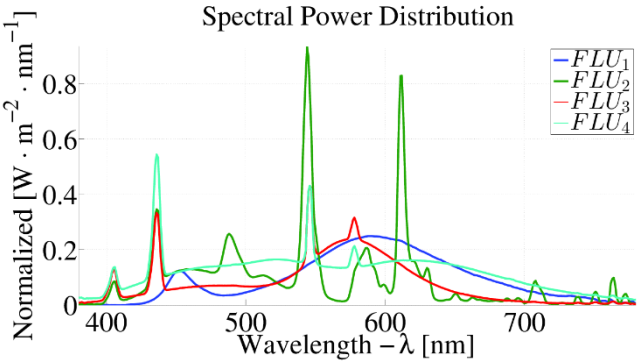

Figure 5. SPD Fluorescent sources.

In Figure 6, four samples of incandescent light sources are shown. The minimum CRI was 93 and the maximum 99. The spectra of incandescent light sources are characterized as being soft and having a significantly high component in the infrared spectrum. The infrared part of their spectrum causes their energy inefficiency, but on the other hand, these light sources exhibit a high color reproducibility. It is also important to know that incandescent light sources have the closest spectrum to the SPD of the Sun.

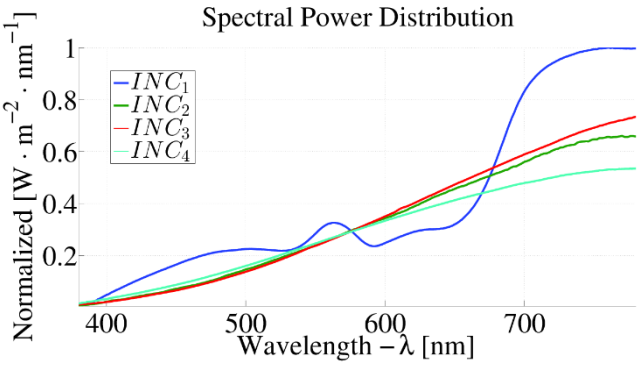

Figure 6. SPD Incandescent sources

Figure 7 shows four samples of LED sources. The minimum CRI was 70 and the maximum 93. All LEDs characterized in this work are white light sources. The white LED sources are constructed

by combining (overlapping) several types of LEDs, these LEDs are overlapped to obtain a white response according to the manufacturers' standards. One of the possibilities of future work, based on the results of this work, is to control a LED light source to match a polychromatic illumination system where the CCT and CRI cannot be controlled. Such initiatives have already been described [26–30], but now they can be studied with greater depth and can focus on particular problems.

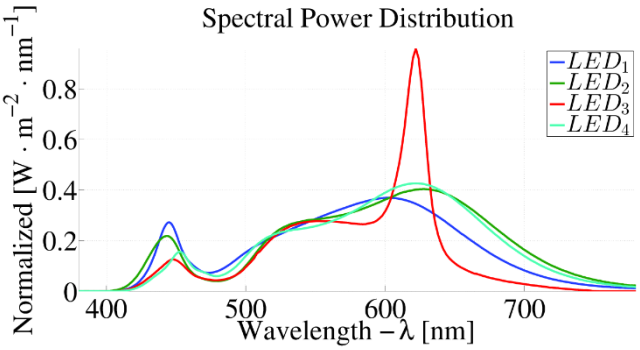

Figure 7. SPD LED sources

IV. EXPERIMENTAL RESULTS

a. Classification

Figure 8 depicts the distribution of the data read by the RGB sensor TCS3414CS. The data was normalized to 8 bits. The RGB values for both sensors and SPD were collected in parallel. The data of the LED and incandescent light sources exhibit a high similarity.

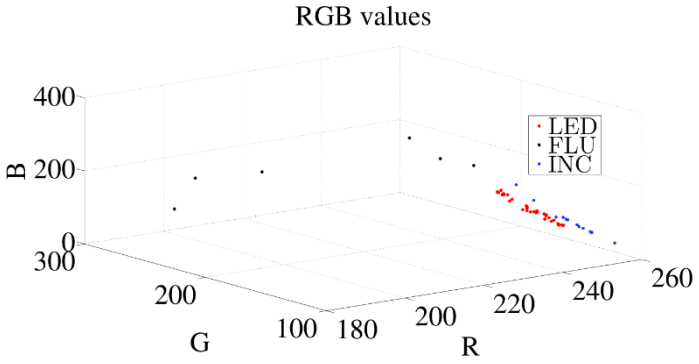

Figure 8. RGB values TCS3414CS

Figure 9 shows the distribution of the data read by the RGB sensor ADJDS311. The data was normalized to 8 bits. The data of the LED and incandescent light sources also exhibit a high

similarity here, but this sensor's readings show a better separation between the LED class and the incandescent class.

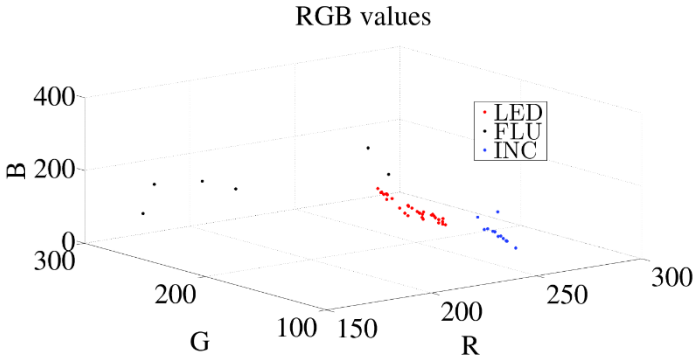

Figure 9. RGB values ADJDS311

Four datasets were constructed to classify the light sources and estimate the CRI values. RGB1, corresponds to the channels R, G, B of the sensor TCS3414CS, RGB2 corresponds to channels R, G, B of the sensor ADJDS311, RGBE1 is RGB1 extended with G/B and R/B for the sensor TCS3414CS and RGBE2 is RGB2 extended with G/B and R/B for the sensor ADJDS311. Table 3 shows the average Mean Squared Error (MSE) and standard deviation of the implemented classifiers. The mean and standard deviation errors are shown for each classifier because each of them is trained with half of the data (randomly selected). The remaining data is used for the actual testing. This test improves the convergence analysis of the classifiers and reduces the possibility of over-fitting the data. In Table 3, LDF is the Linear Discriminant of Fisher, KNN is the K-Nearest Neighbor, SVM is the Support Vector Machine (Polynomial Kernel) and NN is the Neural Network (Perceptron) with Levenberg–Marquardt algorithm. Table 3 shows that KNN performs best with an error of 2.47 %. While the error is equal to the NN in RGBE2 set, the standard deviation is higher. In addition, it is clearly shown that the RGB2 sensor performs better.

Table 3. Classification error

	Fisher	**KNN**	**SVM**	**NN LVM**
RGB1 μ	0.0667	0.0444	0.0630	0.0531
RGB1 σ	0.0381	0.0308	0.0319	0.0850
RGB2 μ	0.0346	**0.0247**	0.0420	0.0407
RGB2 σ	0.0350	0.0297	0.0453	0.0417
RGBE1 μ	0.0568	0.0407	0.0630	0.0654
RGBE1 σ	0.0333	0.0393	0.0414	0.0800
RGBE2 μ	0.0346	**0.0247**	0.0346	0.0247
RGBE2 σ	0.0307	0.0281	0.0350	0.0327

The classification was implemented in order to examine a separate model for each type of source. The model transformations between the RGB space and the CRI value are clearly not linear; however, the proximity of the sources of the same class can adjust a model to a linear response. Table 4 shows the mean square error of the regression implemented for the LED class. For three sources two regression models were implemented, one linear and another one with RBF. The variable k in Table 4, Table 5 and Table 6 represents the number of centroids in the hidden layer of the RBF. The same four data sets, developed in the classification stage, were used, namely RGB1, RGB2, RGBE1 and RGBE2. Table 4 shows that the increase in the number of centroids reduces the error gradually, and that there was no significant improvement using extended datasets.

Table 4. Regression error of the LED class

k	5	10	15	20	25
RGB1 Linear	0.0495	0.0495	0.0495	0.0495	0.0495
RGB1 RBF	0.0432	0.0388	0.0311	0.0188	0.0136
RGB2 Linear	0.0489	0.0489	0.0489	0.0489	0.0489
RGB2 RBF	0.0409	0.0345	0.0272	0.0241	0.0097
RGBE1 Linear	0.0463	0.0463	0.0463	0.0463	0.0463
RGBE1 RBF	0.0447	0.0379	0.0262	0.0205	0.0124
RGBE2 Linear	0.0459	0.0459	0.0459	0.0459	0.0459
RGBE2 RBF	0.0416	0.0350	0.0269	0.0176	0.0157

Table 5 shows the estimation error (MSE) using the linear and the RBF models for the fluorescent class. It is important to note that fewer centroids are required to converge the error to an acceptable level. Again, the error gradually reduces with the increase of the centroids.

Table 5. Regression error of the FLU class

k	2	4	6
RGB1 Linear	0.0355	0.0355	0.0355
RGB1 RBF	0.0807	0.0330	0.0000
RGB2 Linear	0.0484	0.0484	0.0484
RGB2 RBF	0.0772	0.0129	0.0000
RGBE1 Linear	0.0000	0.0000	0.0000
RGBE1 RBF	0.0930	0.0330	0.0000
RGBE2 Linear	0.0000	0.0000	0.0000
RGBE2 RBF	0.0772	0.0119	0.0000

Table 6 demonstrates the estimation error (MSE) using the linear and the RBF models for the incandescent class. It is important to note that fewer centroids are required to converge the error to an acceptable level.

Table 6. Regression error of the INC class

k	2	4	6
RGB1 Linear	0.0099	0.0099	0.0099
RGB1 RBF	0.0087	0.0083	0.0072
RGB2 Linear	0.0109	0.0109	0.0109
RGB2 RBF	0.0112	0.0105	0.0018
RGBE1 Linear	0.0037	0.0037	0.0037
RGBE1 RBF	0.0081	0.0075	0.0015
RGBE2 Linear	0.0112	0.0112	0.0112
RGBE2 RBF	0.0101	0.0096	0.0017

Additionally, with the same data, the CCT was estimated. In **Table 7** the estimation error using the linear model is shown. The RBF estimation was not implemented due to a lower error.

Table 7. Regresion error CCT estimation

	LED	FLU	INC
RGB1	0.0155	0.0141	0.0057
RGB2	0.0265	0.0651	0.0299
RGBE1	**0.0128**	**0.0101**	**0.0029**
RGBE2	0.0184	0.0111	0.0232

V. CONCLUSION

In this paper, we present a classification model of artificial light sources and individual models, constructed to estimate the CRI sources, considering their class using typical low-cost RGB sensors. As part of this work, several light sources commonly used in residential and commercial environments were characterized and the information provided by the manufacturers was corroborated. The results show that the best classifier was the KNN (MSE<3.4 %), and globally, the best estimator was the RBF with MSE < 1.4 %.

The calculation and estimation of these parameters are developed to improve the design of intelligent residential lighting systems and of automatic color measurement to close the control loop in polychromatic light sources. The CRI provides critical information that can also be used to characterize work-spaces and serve as a tool in architectural and lighting design.

By replacing a spectrometer or colorimeter with a low-cost RGB sensor and by constructing simple estimation models, the complete implementation of intelligent systems is possible. This contributes to the improvement in lighting quality and reduces the energy consumption by using hybrid systems (natural and artificial light) or polychromatic light sources.

VI. Acknowledgments

This work is part of the research project “Design and implementation of an intelligent control system with balanced natural light to reduce energy consumption in buildings" with ID P12204, of the Automática, Electrónica y Ciencias Computacionales Group COL0053581. Instituto Tecnológico Metropolitano, Medellín-Colombia. The authors thank CODI, “estrategia de sostenibilidad 2014-2015 from Universidad de Antioquia” for the support to develop this work.

REFERENCES

[1] M. Ashe, D. Chwastyk, C. de Monasterio, M. Gupta, M. Pegors, 2010 U .S. Lighting Market Characterization, 2012.

[2] P.J. Bouma, Physical Aspects of Colour: An Introduction to the Scientific Study of Colour Stimuli and Colour Sensations, (1948) 312.

[3] M.S. Rea, J.P. Freyssinier-Nova, Color rendering: A tale of two metrics, Color Res. Appl. 33 (2008) 192–202. doi:10.1002/col.20399.

[4] G. Sharma, Digital Color Imaging: Handbook, CRC Press, Boca Raton, 2003.

[5] Á. Borbély, Á. Sámson, J. Schanda, The concept of correlated colour temperature revisited, Color Res. Appl. 26 (2001) 450–457. doi:10.1002/col.1065.

[6] G. De Graaf, R.F. Wolffenbuttel, Optical CMOS sensor system for detection of light sources, Sensors Actuators A Phys. 110 (2004) 77–81. doi:10.1016/j.sna.2003.10.046.

[7] C.S. McCamy, Correlated color temperature as an explicit function of chromaticity coordinates, Color Res. Appl. (1992) 142–144.

[8] G. He, J. Xu, H. Yan, Spectral optimization of warm-white light-emitting diode lamp with both color rendering index (CRI) and special CRI of R9 above 90, AIP Adv. 1 (2011) 032160. doi:10.1063/1.3644342.

[9] N. Thejokalyani, S.J. Dhoble, Novel approaches for energy efficient solid state lighting by RGB organic light emitting diodes – A review, Renew. Sustain. Energy Rev. 32 (2014) 448–467. doi:10.1016/j.rser.2014.01.013.

[10] K.A.G. Smet, W.R. Ryckaert, M.R. Pointer, G. Deconinck, P. Hanselaer, A memory colour quality metric for white light sources, Energy Build. 49 (2012) 216–225. doi:10.1016/j.enbuild.2012.02.008.

[11] K.-C. Lee, S.-H. Moon, B. Berkeley, S.-S. Kim, Optical feedback system with integrated color sensor on LCD, Sensors Actuators A Phys. 130-131 (2006) 214–219. doi:10.1016/j.sna.2006.01.028.

[12] J.S. Bajić, D.Z. Stupar, B.M. Dakić, M.B. Živanov, L.F. Nagy, An absolute rotary position sensor based on cylindrical coordinate color space transformation, Sensors Actuators A Phys. 213 (2014) 27–34. doi:10.1016/j.sna.2014.03.036.

[13] T. Fu, Z. Yang, L. Wang, X. Cheng, M. Zhong, C. Shi, Measurement performance of an optical CCD-based pyrometer system, Opt. Laser Technol. 42 (2010) 586–593. doi:10.1016/j.optlastec.2009.10.008.

[14] M. Assaad, I. Yohannes, A. Bermak, D. Ginhac, F. Meriaudeau, Design and characterization of automated color sensor system, Int. J. Smart Sens. Intell. Syst. 7 (2014) 1–12.

[15] H. Escid, M. Attari, M. Ait, W. Mechti, 0 . 35 μm CMOS optical sensor for an integrated transimpedance circuit, Int. J. Smart Sens. Intell. Syst. 4 (2011) 467–481.

[16] K. Ogawa, S. Suzuki, M. Sonehara, T. Sato, K. Asanuma, Optical probe current sensor module using the Kerr effect and its application to IGBT switching current measurements, Int. J. Smart Sens. Intell. Syst. 5 (2011) 594–598. doi:10.1109/ICSensT.2011.6137050.

[17] A. Pandharipande, D. Caicedo, Daylight integrated illumination control of LED systems based on enhanced presence sensing, Energy Build. 43 (2011) 944–950. doi:10.1016/j.enbuild.2010.12.018.

[18] J.S. Sandhu, A.M. Agogino, A.K. Agogino, Wireless sensor networks for commercial lighting control: decision making with multi-agent systems, in: AAAI Work. Sens. Networks, Citeseer, 2004: pp. 131–140.

[19] M. Ashibe, M. Miki, T. Hiroyasu, Distributed optimization algorithm for lighting color control using chroma sensors, in: 2008 IEEE Int. Conf. Syst. Man Cybern., IEEE, Singapore, 2008: pp. 174–178. doi:10.1109/ICSMC.2008.4811270.

[20] J.-S. Botero V., F.-E. López G., J.-F. Vargas B., Calibration method for Correlated Color Temperature (CCT) measurement using RGB color sensors, in: Image, Signal Process. Artif. Vis. (STSIVA), 2013 XVIII Symp., IEEE, Bogotá, 2013: pp. 3–8. doi:10.1109/STSIVA.2013.6644921.

[21] J.-S. Botero V., F.-E. López G., J.-F. Vargas B., Calibration Method for Measuring the Color Rendering Index (CRI) using RGB Sensor, Tecnológicas. EE (2013) 325–338.

[22] M. Yu, Intelligent neural network control strategy, Int. J. Smart Sens. Intell. Syst. 8 (2015) 1406–1423.

[23] J. Qi, J. Cai, Error modeling and compensation of 3d scanning robot system based on pso-rbfnn, Int. J. Smart Sens. Intell. Syst. 7 (2014) 837–855.

[24] CIE, Selected Colorimetric Tables, (2013).

[25] J.S. Botero V., L.G. Morantes G., Estimación de distancia con sensores ópticos reflexivos usando redes neuronales con funciones de base radial para aplicaciones embebidas, Ing. Y Univ. 17 (2013) 27–40.

[26] R. Srividya, C.P. Kurian, White light source towards spectrum tunable lighting — A review, in: IEEE (Ed.), 2014 Int. Conf. Adv. Energy Convers. Technol., IEEE, Manipal, 2014: pp. 203–208. doi:10.1109/ICAECT.2014.6757088.

[27] M. Aldrich, Dynamic Solid State Lighting, Massachusetts Institute of Technology, 2010.

[28] M. Aldrich, N. Zhao, J.A. Paradiso, Energy efficient control of polychromatic solid state lighting using a sensor network, in: SPIE 7784, Tenth Int. Conf. Solid State Light., SPIE, 2010. doi:10.1117/12.860755.

[29] M. Aldrich, A. Badshah, B. Mayton, N. Zhao, J.A. Paradiso, Random walk and lighting control, in: 2013 IEEE Sensors, IEEE, Baltimore, 2013: pp. 1–4. doi:10.1109/ICSENS.2013.6688590.

[30] S. Afshari, S. Mishra, A. Julius, F. Lizarralde, J.D. Wason, J.T. Wen, Modeling and control of color tunable lighting systems, Energy Build. 68 (2014) 242–253. doi:10.1016/j.enbuild.2013.08.036.